Silicon self-interstitial migration paths and barrier energies by the critical-path method

1993 J. Phys.: Condens. Matter 5 6387

(http://iopscience.iop.org/0953-8984/5/35/005)

J. Phys.: Condens. Matter 5 (1993) 6387–6406. Printed in the UK

Silicon self-interstitial migration paths and barrier energies by the critical-path method

K Kato

Advanced Research Laboratory, Research and Development Centre, Toshiba Corporation, 1 Komukai Toshiba-cho, Saiwai-ku, Kawasaki 210, Japan

Received 19 February 1993, in final form 20 April 1993

Abstract. Silicon self-interstitial migration paths and barrier energies have been investigated based on a first-principles critical-path calculation for atomic motions. Self-interstitials are moved through critical paths corresponding to the lowest-energy configurations for thermal diffusion. The results suggest that self-interstitial diffusion occurs mainly as a combination of interstitial-interchange and direct-interstitial mechanisms and that migration begins from stable hexagonal and tetrahedral configurations. The interstitialcy-interchange mechanism has been found to occur only rarely, because the structure becomes unstable when it attempts to move. The calculated migration barrier energies range from 1 eV to a little more than 2 eV, lying at the middle of widely ranging experimental results. Migration through the interstitial-interchange mechanism with a relatively low energy barrier compared with defect generation is attributed mainly to a successive bond remaking process.

1. Introduction

Self-interstitial migration is an interesting subject not only from the viewpoint of basic science but also as a technological issue. Since there is experimental evidence that self-interstitials greatly enhance or retard dopant diffusion in semiconductors [1], self-interstitial migration in semiconductors could be a major obstacle to further integration of silicon technology. In order to make more progress in advanced device technology, self-interstitial migration should be fully understood.

There have been extensive experimental and theoretical studies on self-interstitial migration in semiconductors. Self-interstitial migration has been observed even at cryogenic temperatures in irradiated silicon [2]. This result was explained in terms of the athermal migration of excited Si^0 and Si^{2+} as self-interstitials from tetrahedral to hexagonal sites and vice versa, as revealed by Green-function total-energy calculations [3–8].

Although the proposed mechanism gave many clues to the self-interstitial migration behaviour, experimental results at high temperatures have shown contradicting aspects of self-interstitial migration. Radioactive tracer measurements [9] and gold diffusion experiments [10] confirmed that the silicon self-interstitial diffusion coefficient was rather small compared with group III and V dopant diffusion [11]. The activation energy for diffusion is nearly equal to 5 eV, where the activation energy is mostly dominated by the self-interstitial formation energy. Recent experimental results for extrinsic conditions, however, indicate that the silicon self-interstitial diffusion coefficient is extremely high, about 10 orders higher than that of self-diffusion. The migration energy for diffusion has also been estimated to be as small as 0.13 eV to more than 2 eV [12]. The diffusion

0953-8984/93/356387+20$07.50

of smaller impurities is greatly enhanced by the presence of self-interstitials through an atom-interchanging migration mechanism [13, 14].

To gain a universal understanding of silicon self-interstitial migration, we have to assume that a substitutional/interstitialcy-interchange or substitutional/interstitial-interchange mechanism dominates self-interstitial diffusion in silicon. This paper calls these interstitialcy-interchange and interstitial-interchange mechanisms. Theoretical studies based on a total-energy density-function calculation [15–17] suggest that the migrations caused by these mechanisms are likely to occur because the total-energy difference along the migration path between the configurations is sufficiently small—as low as 0.4 eV. This value is smaller than the theoretical [18] and experimental [19] atom migration energies on silicon surfaces of 0.6 eV parallel to the dimer rows and of 1.0 eV perpendicular to the dimer rows. The experimental migration energies in bulk silicon, however, range widely from 0.13 eV to more than 2 eV because of the experimental difficulties in direct measurement. It is also not clear whether the interstitialcy-interchange or interstitial-interchange mechanism predominates in the diffusion processes [1]. These ambiguities stimulated us to study the self-interstitial migration process in silicon in more detail with accurate calculation.

In this study, a critical-path calculation based on the first-principles density-function theory has been performed, searching for the most probable migration path including saddle points and the associated migration barrier. Since migration paths and barriers strongly depend on the initial conditions of the atom's location and its vibration energy because of finite temperature, there are infinite possibilities for self-interstitial migration paths. Here, a critical-path method is presented to find the lowest-barrier path, because the activation energy for migration is mostly determined by the lowest-barrier path [20, 21]. In section 2, a calculation method involving atomic motion is described. Section 3 presents the results on stable self-interstitial configurations and self-interstitial diffusion mechanisms. Section 4 discusses the results in more detail. Section 5 concludes this paper.

2. Calculation methods

The essential idea of the present calculations is that electronic state calculations are converged at each atom motion step, and that atoms are moved on the well defined Born–Oppenheimer potential-energy surface with slight constraints, and are passed through the saddle configuration on the potential-energy surface.

2.1. Electronic states

The electronic-state calculations are performed using self-consistent pseudopotential techniques within density-functional formalism in the local-density approximation. Fictitious time derivatives of the electronic wavefunctions corresponding to the occupied states are integrated as dynamical freedoms with fictitious masses by the following equation [22, 23]:

$$\mu\ddot{\psi}_{ik}(r,t) = -\frac{\delta E}{\delta \psi^*_{ik}(r,t)} + \sum_j \Delta^k_{ij}(t)\psi_{jk}(r,t) \tag{1}$$

where μ, ψ and E are the fictitious electron mass, the electronic wavefunction and the density-functional energy function, respectively. The Lagrange multipliers Δ^k_{ij} are determined by orthonormality conditions on the wavefunctions. In order to eliminate the computer-intensive work needed for a rigorous treatment of off-diagonal matrix elements,

the Gram–Schmidt orthonormalization scheme [24] has been implemented at each fictitious time step to free the calculation from off-diagonal matrix elements. In simulating the atomic motion, the second derivative of the wavefunction is replaced by a first-derivative equation, using a conjugate gradient minimization scheme [25]. This process reduces CPU time.

The norm-conserving pseudopotential has been employed on the basis of s, p and d *atomic orbitals obtained by following the method by Hamman et al* [26]. The Perdew–Zunger [27] and Ceperley–Alder [28] correlation has been implemented. Since the wavefunctions are expanded by the number of N plane waves, the diagonalization of $N \times N$ consumes substantial CPU time, even if a fictitious time scheme is employed. A total of N^2 operations will be required especially in the implementation of the norm-conserving pseudopotential, because the matrix elements of non-local terms cannot be expressed as a function of wavevector differences. To reduce the number of operations, the non-local potential contribution to energies and forces is divided at the projection operators with the aid of the Kleinman–Bylander scheme [29] before expanding into plane waves [30]. The contribution is, therefore, re-expressed in the square form of N operations. This process together with the application of convolution to the fictitious time integration pushes the most computer-intensive work into a fast Fourier transformation (FFT) of wavefunctions and potentials, which can be fulfilled by $N \times \log N$ operations. Although FFT gives a substantial advantage to vectorized computation, a Fourier transformation defined on M^3 mesh points in three-dimensional space requires $3 \times M^3$ FFT operations along each coordinate axis, resulting in enormous calculation time. This burden is eased if the calculation procedure is completely vectorized. In this paper, each operation in a single FFT along one axis is vectorized with FFT operations along parallel axes on the plane normal to these axes. This procedure improves the vectorized computation efficiency, nearly reaching the potential maximum speed of a vectorized system. The electronic state calculations are performed using $2k$ points from the Chadi–Cohen scheme [31].

2.2. *Supercell and energy cut-offs*

The choice of supercell size affects the calculated energies, because defects in neighbouring small cells can interact with each other. Test calculations are performed for Si^0 and Si^{2+} self-interstitials in 17- and 33-atom cells. The coordinate axes are along the [110], [$\bar{1}$10] and [001] directions. The stable configurations and migration pathways obtained for a 17-atom cell have almost the same result as with a 33-atom case. The total-energy difference of stable configurations for the Si^{2+} case had a discrepancy of 0.3 eV compared with the 33-atom case. The stable bond-centred configuration for Si^0 in a 17-atom cell was more deformed from that in a 33-atom cell. This structure difference results in energy decrease in the 17-atom case. The supercell geometry of 33 atoms including a self-interstitial is, therefore, used in this study to obtain accurate migration energies. To come to a judicious choice and quantitatively reliable results, the dependence on energy cut-offs has been carefully studied, following the method for accurate energy calculation [32–34]. Although the total-energy difference of stable configurations for the Si^0 case showed a rapid convergence with the cut-off energy, the total-energy difference of stable configurations for the Si^{2+} case showed a slow convergence with cut-off energy. Figure 1 shows the convergences of the total-energy difference of bond-centred and split configurations with respect to the tetrahedral configuration for Si^{2+} as a function of the cut-off energy. Here, the total-energy differences of bond-centred and split configurations with respect to the tetrahedral configuration for Si^{2+} were chosen because of their slower convergence with the cut-off energy compared with Si^0 cases. Since the total-energy difference converges at the cut-off energy of 11 Ryd, the cut-off energy of 11 Ryd is sufficient to calculate the migration barrier energies. Stable

configurations and migration barrier energies were calculated with the cut-off energy of 11 Ryd throughout this work.

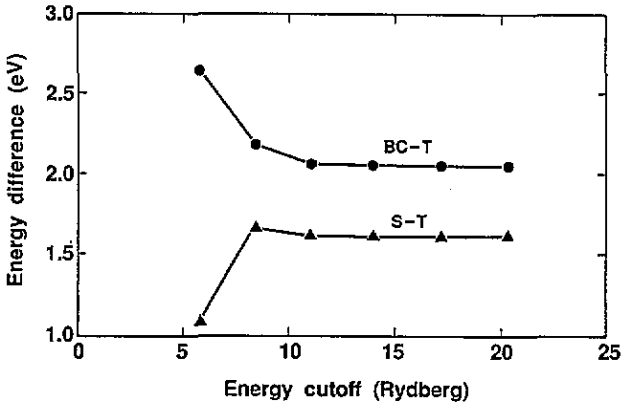

Figure 1. Convergences of total-energy difference of bond-centred and split configurations with respect to the tetrahedral configuration for Si^{2+} as a function of cut-off energy.

2.3. Atomic motion

The main interest is the basic mechanism of diffusion, which is a consequence of successive elemental migration processes. What is needed to understand this mechanism is the elemental process of self-interstitials. A self-interstitial is moved from one stable configuration to another, and this is seen as an elemental diffusion process. Before starting the migration of a self-interstitial atom, a stable configuration for the self-interstitial site is found by removing energy from the system through lattice relaxation from a highly symmetric configuration.

This paper shows the results of careful attention to a rigorous treatment for evaluating the activation energy corresponding to the minimum energy for a self-interstitial migration. At high temperatures, thermal lattice vibrations create a variety of self-interstitial migration pathways. The transition with the lowest migration energy among these processes can be found by pushing the self-interstitial up along the valley through the saddle configuration on the potential-energy surface from a stable configuration and by pushing it down on the potential-energy surface, while moving the remaining atoms into the lowest-energy configuration at each time step. The path through the saddle configuration corresponds to a critical path for diffusion to occur in a system. The activation energy for state transition in a system is the potential-energy difference between the saddle and stable configurations, as proved by the transition-state theory [20]. Once the final configuration for the diffusion process has been determined, the self-interstitial initiating a minimum-barrier migration process is found by pushing it up along the valley on the potential-energy surface towards the saddle point, and by moving over the lowest-energy ridge on the potential-energy surface, as shown in figure 2. There may be further saddle configurations that can be derived from the original configuration. The transitions across these configurations, however, must overcome the higher energy barriers in the initial migration stage before the self-interstitial passes through the saddle configuration. One could expect that self-interstitials rarely jump over a higher energy barrier to reach another saddle point.

The shape of the potential-energy surface for a self-interstitial atom can be derived from the Hellmann–Feynman force given by

$$F = -\sum_{k,i} \left\langle \psi_{ki} \left| \frac{\partial V_{ps}}{\partial R} \right| \psi_{ki} \right\rangle \tag{2}$$

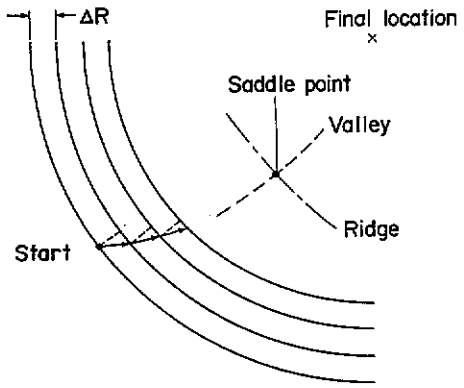

Figure 2. Atom motion scheme on the potential-energy surface to find the minimum-energy barrier. The atom is moved ΔR towards the final location and a corrective motion δR is added.

where V_{ps} and R are pseudopotentials for the self-interstitial and the position vector for a self-interstitial atom, respectively. When the self-interstitial climbs up along the valley on the potential-energy surface, the direction of the force acting on the self-interstitial is exactly opposite to its direction of movement. At each time step shown in figure 2, the self-interstitial is moved one step ΔR towards the final stable location, and then a corrective motion perpendicular to the original motion ΔR is added in proportion to the Hellmann–Feynman force as given by δR,

$$\delta R \propto F - \frac{(F, \Delta R)\Delta R}{|\Delta R|^2}. \tag{3}$$

This procedure puts a slight constraint on the self-interstitial motion, forcing the self-interstitial to avoid higher potential hills and to drop inevitably into the valley on the potential-energy surface. This process is like finger-pushing an object on the potential-energy surface. This can be extended to find a saddle point in an arbitrary n-dimensional space. The other atoms up to the second-nearest neighbours of the self-interstitial are allowed to relax according to Hellmann-Feynman forces at each time step to obtain the energy-minimum saddle configuration. Relaxation of further-neighbour shells may reduce the stored energy. The consequences of these additional relaxations for the migration energy have not yet been investigated in the literature. Migration energies are calculated as energies of saddle configurations with respect to the initial stable configurations.

The motion of Si^{2+} was traced between two adjacent tetrahedral sites on the same (001) plane to confirm whether the scheme works well in order to find the minimum-barrier path, as shown in figure 3. Tetrahedral sites are the most stable sites for Si^{2+}, while hexagonal sites are saddle points for Si^{2+}, as theoretically examined in prior studies [5]. Si^{2+} deviated from the (001) plane at the initial stage, passing through the hexagonal saddle configuration and tetrahedral and hexagonal configurations successively, and finally moved into the adjacent tetrahedral site on the original plane, proving that the scheme works well as a way to find the pathway with the lowest energy barrier.

3. Results

The results of following the atomic motion are described in this section, as an atom starts from one stable configuration and moves to another. The pathway and the migration energy needed for interstitialcy-interchange, interstitial-interchange and direct-interstitial mechanisms are studied. Since elemental semiconductors such as silicon have a rather

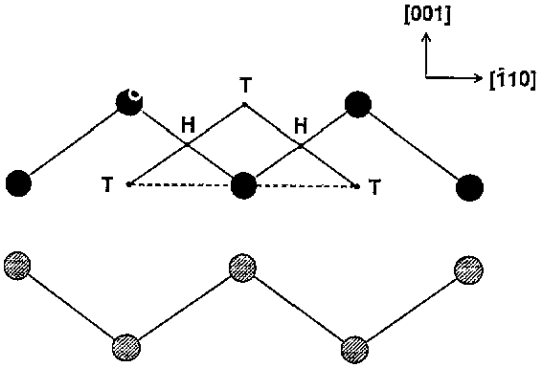

Figure 3. Obtained trajectory of Si^{2+} motion from tetrahedral through hexagonal sites by using the present scheme. Atoms located on and below the plane are denoted by full and hatched circles, respectively.

loosely packed lattice, there exists not only an ideal interstitial but also an interstitialcy, self-interstitial atoms forming bridges between adjacent host atoms. These different types of structure can also be distinguished during atom migration, because migration processes occur in different ways. Assuming that both types of structure exist in atom-interchanging migration processes, one could discriminately define interstitialcy-interchange and interstitial-interchange mechanisms according to interstitialcy and interstitial migrations, respectively [1, 35]. For direct self-interstitial migration, this paper simply calls it the direct-interstitial mechanism. First, stable configurations including a self-interstitial were found from several highly symmetric configurations. Then, the elemental migration processes were investigated, starting from these initial stable configurations.

3.1. Stable configuration

Total-energy density-function calculations for Si^0 and Si^{2+} have been performed, which were proved to be the lowest-energy states for n-type and p-type silicon, respectively [5], because of the negative U system. The migration of deeper Si^+ was not examined, because it is not the lowest charged state in the stable tetrahedral and hexagonal configurations. Migration by Si^+ will quickly transform Si^+ into stable Si^0 and Si^{2+}, even if it exists as an intermediate structure. A uniform background charge is added to neutralize the system for the Si^{2+} calculation [15–17]. All atoms up to the second-nearest neighbours of a self-interstitial are gradually relaxed into the lowest-energy structure for the system with an additional self-interstitial atom on hexagonal, tetrahedral, split and bond-centre sites in a perfect crystal structure.

A schematic representation of stable configurations obtained from calculations is shown in figure 4. Hexagonal, split and bond-centred configurations are stable for Si^0 self-interstitials, while tetrahedral, split and bond-centred configurations are stable for Si^{2+} self-interstitials. Both split and bond-centred configurations have been found to be stable. It must be noted that atom configurations for different charged states are different from each other, because the atoms are relaxed. The configurations for Si^0 self-interstitials are not completely symmetric because of the existence of dangling bonds. The self-interstitial sites are slightly deformed from a symmetric configuration to reduce the total energy. The distance between split sites after lattice relaxation was 2.07 Å. This value is smaller than the normal bond length of 2.35 Å in a perfect crystal, but slightly larger than the distance of 2.05 Å between the split sites for Si^{2+}. This confirms that the bond lengths for Si^0 self-interstitials are slightly longer than those for Si^{2+} cases. This difference presumably contributes to the ion–ion Ewald (electrostatic) energy difference between the cases of Si^0

Table 1. Energy differences (eV) for stable split (S) and bond-centred (BC) configurations from stable hexagonal (H) and tetragonal (T) configurations for Si^0 and Si^{2+}.

	Si^0		Si^{2+}	
Configurations	S–H	BC–H	S–T	BC–T
ΔE_e	21.4	24.0	19.1	19.0
ΔE_s	−20.4	−22.3	−17.5	−16.9
ΔE_t	1.0	1.7	1.6	2.1

and Si^{2+}. The distances between the bond-centre site and its two adjacent nearest sites result in 2.01 Å for Si^0 and 2.01 Å for Si^{2+}.

Table 1 shows the energy differences for stable split and bond-centred configurations found for Si^0 and Si^{2+}, with respect to the most stable hexagonal and tetrahedral configurations. The total-energy differences are divided into electronic energy and electrostatic energy parts. Here, the electrostatic energy E_s of a system is defined by

$$E_s = E_{ii} - E_{ie} + E_{ee} \tag{4}$$

where E_{ii}, E_{ie} and E_{ee} are expressed in Rydberg units by

$$E_{ii} = \frac{1}{2}\sum_{\mu\neq\nu}\frac{2Z_\mu Z_\nu}{|R_\mu - R_\nu|} \tag{5}$$

$$E_{ie} = \sum_\mu \int \frac{2Z_\mu}{|r - R_\mu|}\rho_0\,dr \tag{6}$$

$$E_{ee} = \frac{1}{2}\int\int \frac{2}{|r - r'|}\rho_0^2\,dr\,dr'. \tag{7}$$

Z_μ is the valence of the μth core and R_μ is the position vector of the μth atom. ρ_0 is the average density of valence electrons in the system. The electronic energy E_e is defined by subtracting E_s from the total energy E_t

$$E_e = E_t - E_s. \tag{8}$$

The total-energy differences among hexagonal, split and bond-centred configurations for Si^0 were rather small compared with the total-energy differences for Si^{2+}. The result of the detailed analysis listed in table 1 indicates that the electronic energy for Si^0 increases through a change in the system from a hexagonal configuration to a split configuration, while the electrostatic energy decreases dramatically to compensate for the energy increase due to the electronic states. The electrostatic energy compensation for Si^{2+} is, however, not as conspicuous as is the case for Si^0. Although one cannot reason how these values contribute to the smaller energy increase for Si^0 compared with the Si^{2+} case, the broader atom distribution for the self-interstitial can result in a large electrostatic energy compensation, eventually leading to a smaller energy increase in the Si^0 cases compared with the Si^{2+} cases.

The energies of stable configurations in a supercell geometry comprising 17 atoms have also been calculated to test the effects on total-energy differences by supercell geometries. The stable configurations obtained for the smaller-volume system remained the same. The most stable structure in this case is also a hexagonal configuration for the Si^0 self-interstitial, and is a tetrahedral configuration for the Si^{2+} self-interstitial. Although it is difficult to determine the exact total-energy difference between split and bond-centred configurations because of the small energy difference, the calculated results indicate that hexagonal and tetrahedral configurations are the most stable structures for Si^0 and Si^{2+}, respectively, in this study.

3.2. Interstitialcy-interchange mechanism

The experimental results suggest that the self-interstitial diffusion rate under extrinsic conditions is much higher than the self-diffusion rate, implying that the interstitialcy-interchange or interstitial-interchange mechanism may be predominant in self-interstitial diffusion processes [1]. The interstitialcy-interchange mechanism may occur as transport of a point-defect-modulated structure like a soliton. A plausible structure for intermediate states would be an energetically stable configuration. Among the stable configurations found in this study, the intermediate stable structures are split and bond-centred configurations for both Si^0 and Si^{2+}, because they accompany significant relaxation in adjacent sites. Hexagonal and tetrahedral configurations are not likely to be intermediately stable structures, because relaxation of the nearest-neighbour sites is too small (a few per cent of the bond length) to transport a defect-modulated structure to the next site. Split and bond-centred configurations were chosen as initial structures for interstitialcy diffusion for both Si^0 and Si^{2+} cases.

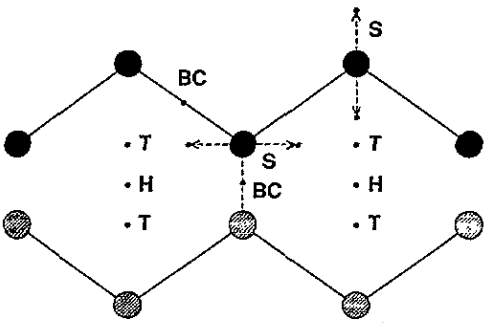

Figure 4. Schematic representation of stable configurations for self-interstitials. Hexagonal, split and bond-centred configurations are stable for Si^0, while tetrahedral, split and bond-centred configurations are stable for Si^{2+}. Atoms located on and below the plane are denoted by full and hatched circles, respectively.

To examine the interstitialcy diffusion mechanism, a self-interstitial atom forming a split site and a bond-centre self-interstitial atom were moved towards the nearest-neighbour lattice site corresponding to an expected lattice site as a final location by passing through a saddle configuration. Here, a finally expected lattice site was chosen as a destination, because a finally expected lattice site is a reasonable final location to transform a deformed structure rather than adjacent atom positions in split and bond-centred configurations. Figure 5 shows the self-interstitial migration processes, starting from (*a*) split and (*b*) bond-centred configurations for the Si^0 case. The relaxation of lattice sites up to the second-nearest neighbours of a migrating atom was also included. The energy barriers for these migrations are summarized in table 2. The atom composing the split site on the left-hand side was driven to a finally expected location close to the centre of the split site through a saddle configuration path, and was stabilized at the lattice site, while the other self-interstitial of the split site on the right-hand side was pushed away by this adjacent self-interstitial and was finally relaxed into a nearest hexagonal site, as shown in figure 5(*a*). The final structure achieved by pushing away the self-interstitial was a hexagonal configuration, and it has a slightly lower energy than the initial structure. The energy barrier of 0.7 eV for the transition implies that the structure is easily changed into an energetically stable hexagonal configuration, rather than transporting the same structure to the next site. Figure 5(*b*) shows that a similar result was obtained for a migration process starting from a bond-centred configuration. The atom located at the bond-centre site was driven to a finally expected location towards the lower adjacent lattice site through a saddle configuration, pushing the lower adjacent atom into a lower-energy configuration. Although the motion by the upper side atom adjacent to the self-interstitial is short, the self-interstitial atom was

finally relaxed into the original lattice site, while the lower adjacent lattice atom was pushed further and relaxed into the nearest hexagonal site. The final structure in this case was also a hexagonal configuration, the same as the result in figure 5(*a*). The energy barrier of 0.2 eV for this transition is again smaller than the value for the split configuration, and is sufficiently low for the structure to change easily from a bond-centred configuration to a hexagonal configuration.

Table 2. Energy barriers (eV) for Si^0 and Si^{2+} migrations from stable split and bond-centred configurations to more stable configurations in trials for the interstitialcy-interchange mechanism.

	Si^0		Si^{2+}	
Path	S→H	BC→H	S→T	BC→T
	0.7	0.2	0.6	0.2

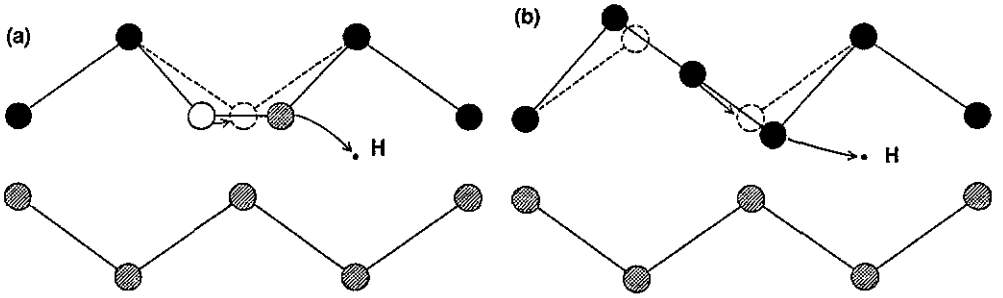

Figure 5. Atom trajectories for self-interstitial migration from (*a*) split and (*b*) bond-centred Si^0 configurations. Atoms located on, above and below the plane are denoted by full, open and hatched circles, respectively.

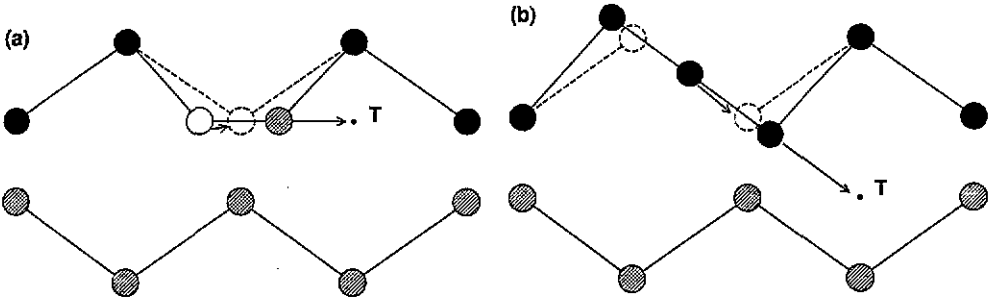

Figure 6. Atom trajectories for self-interstitial migration from (*a*) split and (*b*) bond-centred Si^{2+} configurations. Atoms located on, above and below the plane are denoted by full, open and hatched circles, respectively.

Figure 6 shows the self-interstitial migration processes starting from (*a*) split and (*b*) bond-centred configurations for the Si^{2+} case. The energy barriers for the migrations are summarized in table 2. As shown in figure 6(*a*), the split configuration changed into a

tetrahedral configuration when the atom forming the split site on the left-hand side was driven to a finally expected location towards the centre of the split site and was stabilized at the original lattice site, while the other atom forming the split site on the right-hand side relaxed into the nearest tetrahedral site, as in the case for figure 5(*a*). The final tetrahedral configuration is more stable than the initial structure. The energy barrier for the transition is as low as 0.6 eV, implying that the initial structure easily decays into an energetically favoured tetrahedral configuration. Figure 6(*b*) shows a similar structure change from a bond-centred configuration for Si^{2+} when the atom located at a bond-centre site was driven to a finally expected location towards a lower adjacent original lattice site, pushing the lower adjacent atom towards the lower side. The final structure in this case is also a tetrahedral configuration, the same as in figure 6(*a*). The barrier of 0.2 eV for this transition is sufficiently small to easily allow the transition. The bond-centred configuration, therefore, becomes too unstable when an attempt is made to move it. The structure cannot, therefore, be maintained.

The exploration of plausible migration paths by the interstitialcy-interchange mechanism failed to find a defect-modulated structure transport. If semi-stable structures are given sufficient energy to overcome the energy barriers, rather than passing through critical paths, they may be transported as defect-modulated structures in specific cases. The probability is, however, low because of small energy barriers for relaxation into more stable structures. An accidentally generated semi-stable structure will soon decay into a more stable structure within a few elemental migration processes.

3.3. Interstitial-interchange mechanism

Since the probability of interstitialcy migration is extremely low, as described in the last subsection, the remaining candidate for an atom-interchanging mechanism in migration processes is the interstitial-interchange mechanism. Self-interstitial migration occurs as an energetically activated self-interstitial kicks out a lattice site atom into an adjacent interstitial site. Plausible initial stable structures for the elemental processes in this mechanism are a hexagonal configuration for Si^0 and a tetrahedral configuration for Si^{2+}. Although split and bond-centred configurations may appear as intermediate structures during migration processes from stable sites to stable sites, the initial structure for an elemental process has no choice but a hexagonal configuration for Si^0 and a tetrahedral configuration for Si^{2+}.

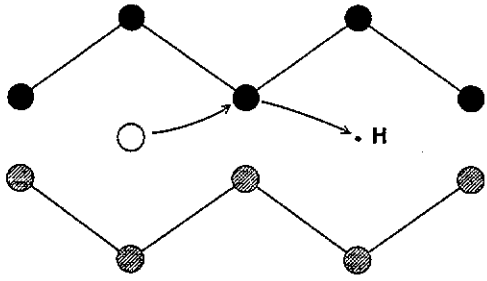

Figure 7. Atom trajectory for self-interstitial migration from the Si^0 hexagonal configuration by the interstitial-interchange mechanism. Atoms located on, above and below the plane are denoted by full, open and hatched circles respectively.

Figure 7 shows the self-interstitial migration from a hexagonal site for Si^0 by passing through a saddle configuration. The self-interstitial on the left-hand side is moved towards one of the four adjacent lattice sites located at the centre of the system, and is stabilized at the lattice site after ejecting the lattice atom. The atom initially located at the centre of the system turns into a self-interstitial and relaxes into one of the two nearest hexagonal sites.

The elemental process for the self-interstitial migration of Si^0 thus ends in the same structure as the initial structure. The energy barrier for this transition is 1.2 eV, as summarized in table 3.

Table 3. Energy barriers (eV) for the interstitial-interchange mechanism starting from the Si^0 hexagonal configuration and from the Si^{2+} tetrahedral configuration.

	Si^0	Si^{2+}
Path	H→X→H	T→X→T
	1.2	2.4

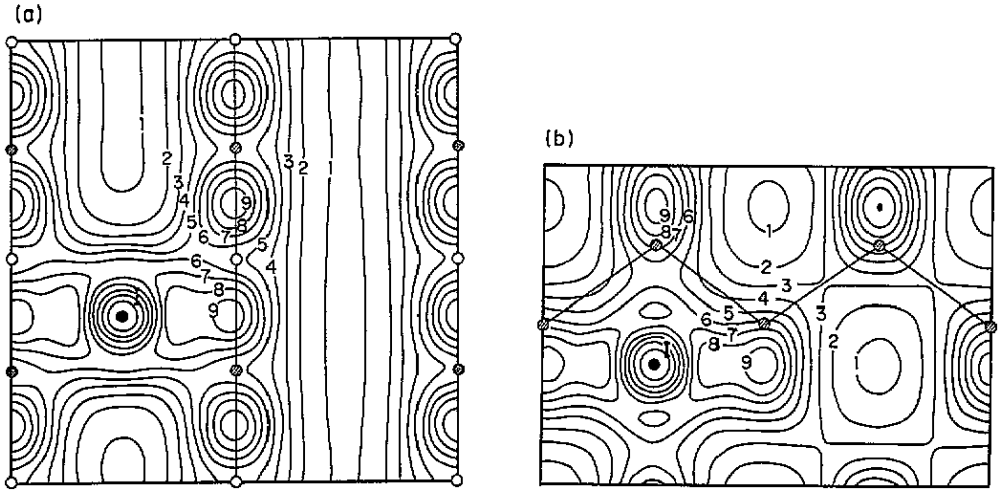

Figure 8. Valence charge density on (*a*) the (001) and (*b*) the ($\bar{1}$10) planes involving the self-interstitial and its adjacent atoms at the initial stage by the Si^0 interstitial-interchange mechanism. Units of density are 10^{-2}/au^3. The self-interstitial is denoted by I. Atoms located on, above and below the plane are denoted by full, open and hatched circles, respectively.

The total valence charge densities at the initial stage and at the atom-interchanging stage during self-interstitial migration are shown in figures 8 and 9, giving the results of investigating the relatively low energy needed to eject an atom compared with the point-defect creation energy. The structures shown here are 17-atom cells. The valence charge density is shown on the two planes involving the self-interstitial and its adjacent atoms, sliced along (*a*) the (001) and (*b*) the ($\bar{1}$10) planes. The charge density at the initial stage shown in figure 8 indicates that the valence electron of a hexagonal self-interstitial is loosely bonded to the two pairs consisting of four adjacent lattice atoms, while adjacent atoms are tightly bonded to their nearest-neighbour lattice atoms. The electronic states do not exceed the band gap at the initial stage shown in figure 8 [16]. As the transition proceeds, the self-interstitial makes bonds with a lower adjacent atom, with an initially lattice-located atom as shown in figure 9(*a*), and with an upper second-nearest-neighbour atom as shown in figure 9(*b*), while the initially lattice-located atom still has bonds with the right-hand-side nearest neighbour (figure 9(*b*)), with the lower side atom (figure 9(*a*)) and with the self-interstitial atom. The upper and lower directions here point in the [001] direction. The

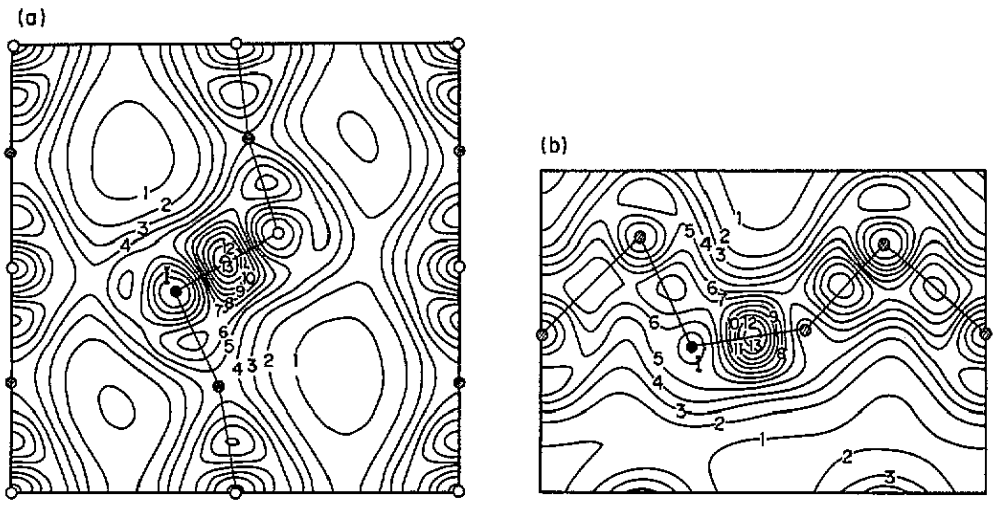

Figure 9. Valence charge density on (*a*) the (001) and (*b*) the ($\bar{1}$10) planes involving the self-interstitial and its adjacent atoms at the atom-interchanging stage by the Si^0 interstitial-interchange mechanism. Units of density are 10^{-2}/au^3. The self-interstitial is denoted by I. Atoms located on, above and below the plane are denoted by full, open and hatched circles, respectively.

original chemical bonds between the two atoms and their neighbour atoms are, thus, rebuilt successively from the initially lattice-located atom to the self-interstitial so as not to increase the energy too much during the atom-interchanging migration process. The saddle point lies in the vicinity of the split configuration, but does not find any semi-stable configuration in this transition. The large relaxation caused by the spatial occupation of dangling bonds at the atom-interchanging stage increases the bond length, and decreases the electrostatic energy as compared with the electronic energy increase. This is considered to be the reason why the gradual bond-remaking process increases the total energy only by a little more than 1 eV and not up to the self-interstitial creation energy.

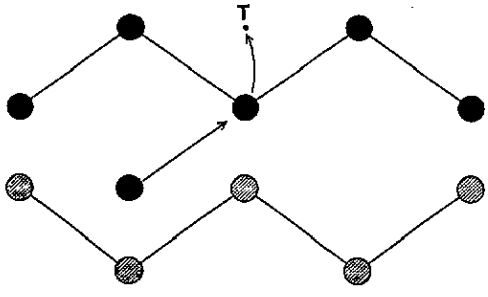

Figure 10. Atom trajectory for self-interstitial migration from the Si^{2+} tetrahedral configuration by the interstitial-interchange mechanism. Atoms located on and below the plane are denoted by full and hatched circles, respectively.

Figure 10 shows self-interstitial migration from a tetrahedral site for Si^{2+}. The self-interstitial on the left-hand side in the system is also moved towards one of the four adjacent lattice sites located at the centre of the system and is stabilized at the lattice site after pushing the lattice atom away, as is the case for Si^0. The atom released from the centre of the system becomes a self-interstitial, and relaxes into one of the two nearest tetrahedral sites. The elemental process of self-interstitial migration for Si^{2+} also ends in the same structure as

the initial structure as in the case for Si^0. The energy barrier for this transition is, however, 2.4 eV as listed in table 3, being relatively higher than that for Si^0.

The total valence charge densities at the initial stage and at the atom-interchanging stage during self-interstitial migration are also shown in figures 11 and 12, indicating the results of investigating the relatively high energy barrier. The sliced planes also involve the self-interstitial atom and its adjacent atoms. The charge density at the initial stage shows that the valence electron of the tetrahedral self-interstitial is loosely bonded to the four adjacent lattice atoms, while the adjacent atoms are tightly bonded to their nearest-neighbour lattice atoms as in the case of Si^0, as seen in figure 11. The charge density near the lattice atoms is relatively low, compared with the case for Si^0. As the transition proceeds, as shown in figure 12, the bonds between the atoms are successively but more rapidly changed from the lattice centre atom to the self-interstitial atom, compared with the case of Si^0. The chemical bonds to two lower atoms (figure 12(*a*)) and the bond to an upper atom (figure 12(*b*)) are almost simultaneously remade by the self-interstitial atom, because the self-interstitial atom moves maintaining nearly the same distance with the two upper atoms. The saddle-point path also lies in the vicinity of the split configuration, but does not find any semi-stable configuration in this transition. Although the electronic energy increase for this case is smaller than in the case of Si^0, the electrostatic energy compensation is not so large as in the case of Si^0. The barrier energies for Si^0 and Si^{2+} diffusions by the interstitial-interchange mechanism correspond roughly to the total-energy differences between the split and the most stable sites for Si^0 and Si^{2+}, as given in section 3.1. The bond length at this atom-interchanging stage for Si^{2+} is, therefore, relatively short because of the lower electron density, resulting in a smaller electrostatic energy compensation and a higher migration barrier.

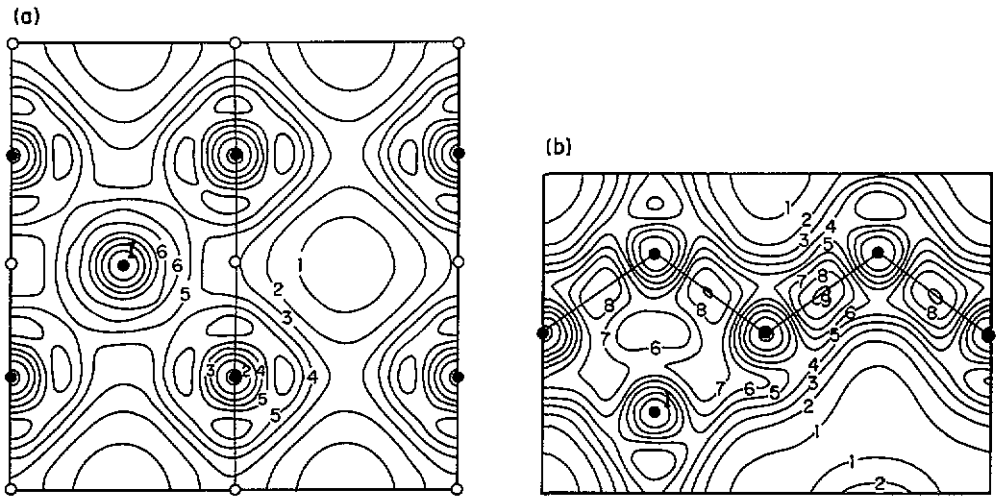

Figure 11. Valence charge density on (*a*) the (001) and (*b*) the ($\bar{1}$10) planes involving the self-interstitial and its adjacent atoms at the initial stage by the Si^{2+} interstitial interchange mechanism. Units of density are 10^{-2}/au^3. The self-interstitial is denoted by I. Atoms located on and above the plane are denoted by full and open circles, respectively.

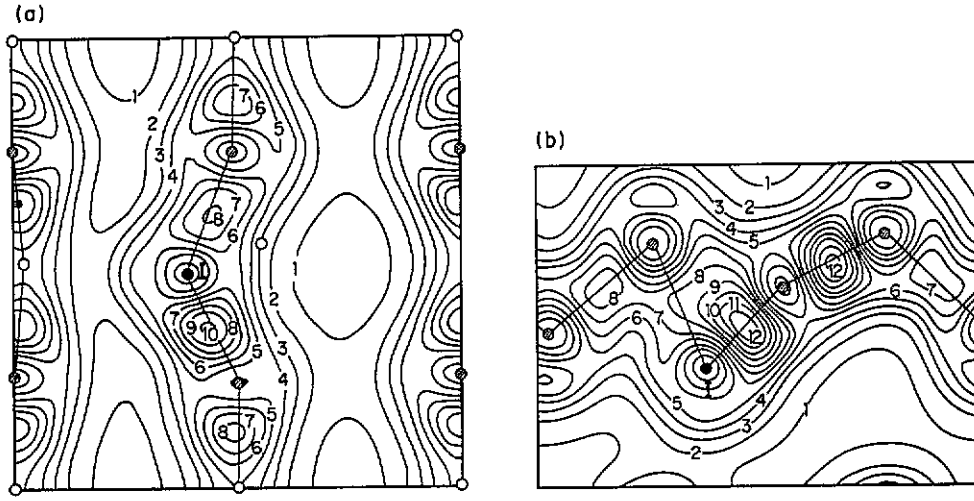

Figure 12. Valence charge density on (*a*) the (001) and (*b*) the ($\bar{1}$10) planes involving the self-interstitial and its adjacent atoms at the atom-interchanging stage by the Si^{2+} interstitial-interchange mechanism. Units of density are $10^{-2}/au^3$. The self-interstitial is denoted by I. Atoms located on, above and below the plane are denoted by full, open and hatched circles, respectively.

3.4. Direct-interstitial mechanism

Since migration by the interstitial-interchange mechanism has been indicated to occur with low energy barriers, this paper focuses on the possible direct-interstitial mechanisms. Here, direct-interstitial mechanism means direct interstitial migration by itself. Several theoretical investigations have shown a direct self-interstitial diffusion from hexagonal to hexagonal sites through a tetrahedral site for Si^0 and tetrahedral to tetrahedral sites through a hexagonal site for Si^{2+} with the energy barrier ranging from 1 to 2 eV for both cases [5, 8, 15]. Except for these mechanisms, direct diffusion from stable to stable sites through a bond-centred configuration may occur accompanied by a large relaxation on the nearest neighbours [17], because the total-energy difference between a bond-centred configuration and a hexagonal or tetrahedral configuration is not so large. These considerations have led to a re-examination of the direct-interstitial mechanism by taking lattice relaxation more into account.

Table 4. Energy barriers (eV) for direct-interstitial mechanisms starting from the Si^0 hexagonal configuration and from the Si^{2+} tetrahedral configuration.

	Si^0		Si^{2+}	
Path	H→T→H	H→BC→H	T→H→T	T→BC→T
	1.2	1.7	1.3	2.3

Table 4 shows the energy barriers for individual direct-interstitial mechanisms. Here, the hexagonal to hexagonal site migration through a bond-centred configuration for Si^0, as shown in figure 13, and the tetrahedral to tetrahedral site migration through a bond-centred configuration for Si^{2+}, as shown in figure 14, are added to the hexagonal to hexagonal site migration through a tetrahedral site for Si^0 and the tetrahedral to tetrahedral site migration

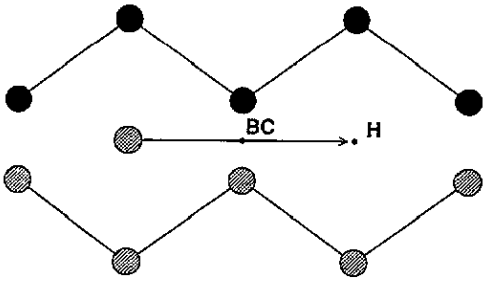

Figure 13. Atom trajectory for self-interstitial migration for Si^0 for a hexagonal to hexagonal site migration through a bond-centred configuration by the direct-interstitial mechanism. Atoms located on and below the plane are denoted by full and hatched circles, respectively.

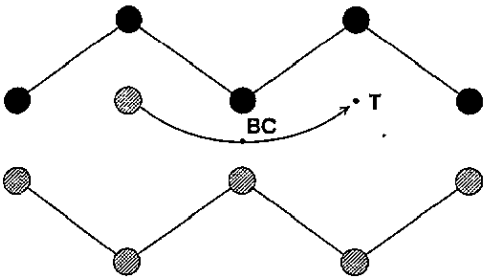

Figure 14. Atom trajectory for self-interstitial migration for Si^{2+} for a tetrahedral to tetrahedral site migration through a bond-centred configuration by the direct-interstitial mechanism. Atoms located on and below the plane are denoted by full and hatched circles, respectively.

through a hexagonal site for Si^{2+}, as shown in figure 3. In the case of Si^0, the energy barrier of 1.2 eV from the hexagonal site through the tetrahedral site and that of 1.7 eV through the bond-centred configuration are comparable with the values for the interstitial-interchange mechanism, and are sufficiently low to allow migration. The energy barrier of 1.3 eV for Si^{2+} through the hexagonal site is far smaller than the value for the interstitial-interchange mechanism. Migrations with a relatively low energy barrier may be attributed to transition processes through bonds with successive bond formation during the process, or to direct diffusion steps of self-interstitials where the latter are loosely bound to adjacent atoms during the transition. In spite of the earlier expectation of interstitial-interchange mechanism predominance, the result suggests that self-interstitial diffusion occurs not only by the interstitial-interchange mechanism but also by the direct-interstitial mechanism. This fact, however, does not contradict the experimental results. A migration mechanism accounting for the experimental results will be discussed in the following section.

4. Discussion

The silicon self-interstitial is one of the most extensively studied defects in solids through both theoretical and experimental approaches, but still has unknown aspects in the migration process. A direct measurement of the self-interstitial diffusion mechanism is impossible because discrimination between direct diffusion and indirect diffusion is difficult in experimental measurements. The behaviour of self-interstitial diffusion can be estimated only through indirect measurements. This is one of the reasons why there is considerable disagreement among experimental results.

Table 5. Experimental migration and activation energies for self-interstitial migration and self-interstitial formation energy (eV).

Migration energy	Activation energy	Formation energy
0.13[a], 0.4[b], 1.2[c], 1.3[d], 1.58[e], 2.0[f], 4.4[g]	5.0[c], 5.01[h]	2.9[i], 3.8[c]

Sources:
[a] [40]. [b] [11]. [c] [39]. [d] [38]. [e] [37]. [f] [36]. [g] [41]. [h] [42]. [i] [43].

Table 6. Energy differences (eV) for split and bond-centred configurations from hexagonal and tetrahedral configurations for Si^0 and Si^{2+} by previous studies.

	Si^0		Si^{2+}		
Configurations	S–H	BC–H	S–T	BC–T	Reference
	1.1	0.0	1.9	0.7	[17]
	—	−0.2	—	0.6	[5]

4.1. Comparison with experiments and previous theories

Table 5 summarizes the experimental migration energies of the self-interstitial obtained by the various techniques reported so far. An earlier study on self-interstitial diffusion suggests that the migration energy for self-interstitial diffusion is estimated to be 0.4 eV from various kinds of experimental data [11]. Experimental results reported later have indicated, though indirectly, that the self-interstitial migration energy is rather high compared with the migration energy of 0.4 eV. The self-interstitial migration energy has been estimated as 2 eV by examining the lateral phosphorus diffusion enhanced by silicon surface oxidation [36]. Oxidation-enhanced diffusion combined with numerical simulation has revealed the self-interstitial migration energy to be 1.58 eV [37]. The time-dependent change in oxidation-enhanced dopant diffusion rate has revealed the migration energy for self-interstitial diffusion to be 1.3 eV [38]. An analysis utilizing combined data from platinum and gold diffusion studies has given 1.2 eV [39]. These experimental analyses involving other experimental results obtained by self-interstitial enhanced phosphorus diffusion [40], and oxygen precipitation and oxidation stacking fault growth [41] suggest that the migration energy widely ranges between 0.13 and 4.4 eV. These results indicate that there still remains widely spread uncertainty in experimental self-interstitial migration energy. The previous theoretical works indicate that the direct-interstitial migration energy depends on the Fermi level [5, 6]. It might have caused some deviation in experimental migration energies. Since the experimental results are mostly obtained using doped silicon, the Fermi-level effects on migration energy should be carefully examined. Insofar as we can tell from the reported experimental results, it cannot be clarified how the Fermi level affects experimental migration energy. Although the theoretical migration energies of 1 eV to a little more than 2 eV obtained in this study lie in between the experimental results, and the recent experimental results are closer to the result of this study, uncertainty in experimental migration energies, however, does not assure validity for accurate calculation.

Another approach to obtain migration energy is to estimate the value from the difference between the activation energy for self-interstitial migration and the self-interstitial formation energy, because the activation energy is divided into the self-interstitial formation part and the self-interstitial migration part. These values obtained by experiments are listed in table 5 [39, 42, 43]. From these results reported so far, the migration energy can be estimated to be 1.2 to 2.1 eV, lying at the middle of the above migration energies reported so far.

Table 7. Energy barriers (eV) for self-interstitial migration starting from the Si^0 hexagonal configuration and from the Si^{2+} tetrahedral configuration by previous studies.

	Si^0		Si^{2+}		
Path	H→T→H	H→X→H	T→H→T	T→X→T	Reference
	1.3	0.4	1.1	1.1	[17]
	1.1	—	1.2	—	[8]

Tables 6 and 7 list the total-energy difference for different configurations and migration energies for some pathways by previous works [5, 8, 17]. Compared with the previous results, both split and bond-centred configurations are stable in the present calculation. The total-energy differences between split and hexagonal configurations for Si^0 and between split and tetrahedral configurations for Si^{2+} in table 1 coincide overall with the previous supercell studies within 0.3 eV error [17]. The total-energy differences between hexagonal and tetrahedral configurations for both charged states are in agreement with the recent Green-function study [8]. It is presumably because lattice relaxation is small in these cases. The total-energy differences between bond-centred and hexagonal configurations for Si^0, and between bond-centred and tetrahedral configurations for Si^{2+}, however, have discrepancies up to 1.7 and 1.4 eV compared with the previous calculated results [8, 17]. The most noticeable difference is that the hexagonal configuration is the most stable for Si^0 in the present calculation, while the bond-centred configuration is also the most stable for Si^0, comparable with the hexagonal configuration in the previous works. It is not likely that this difference arises from pseudopotential differences or integration over the Brillouin zone, because calculations for other configurations are generally in agreement with prior supercell studies. The main differences in the calculation methods between this work and prior supercell studies are the lattice relaxation, the supercell size and the atom motion scheme. The stable configurations found in this work were found by relaxing all atoms up to the second-nearest neighbours of a self-interstitial from a perfect crystal with an additional atom on the bond-centre site. The resulting configurations, therefore, give some differences to this work from the previous work. The total lattice relaxation causes an energy reduction of far more than 1 eV in the present calculation. Although these effects are sufficient to make a difference in the total-energy difference, it may be strange that the total energy of a bond-centred configuration for Si^0 well relaxed in the present calculation becomes relatively higher than those of the previous results. The lattice relaxation alone does not explain the difference in results. The supercell size has some effects on the structure of a bond-centred configuration for Si^0 by changing a 33-atom cell to a 17-atom cell. It might have caused some difference from the previous supercell studies, but may not be sufficient to explain the large difference. The bond lengths between the bond-centred atom and its adjacent atoms in the previous work [17] are seemingly rather long compared with the present study. The total energy of the bond-centred configuration has actually decreased as the bond length is further elongated in this study, but it requires overcoming an energy barrier. These results suggest that the differences in the initial conditions for atom relaxation or the atom motion scheme may have caused the discrepancies.

Compared with previous works carried out by the supercell and the Green-function methods [8, 17], the migration energies for the direct-interstitial mechanism have roughly the same value in the present calculation. This is presumably because the lattice relaxation is not so large in this case. The prior supercell study reported a migration energy of 0.4 eV for Si^0 migration from a hexagonal configuration and of 1.1 eV for Si^{2+} migration from a tetrahedral configuration for the atom-interchanging mechanism [17]. Although the values of 0.4 and 1.1 eV are relatively lower than the present calculation of 1.2 and 2.4 eV, they lie within the widely ranging experimental migration energies listed in table 5. The difference in migration energies for the atom-interchanging mechanism is considered to arise also from the difference in lattice relaxation, supercell size and especially migration pathways. All atoms up to the second-nearest neighbours of a self-interstitial are relaxed in the present calculation. Migrating atoms move over saddle points by passing through critical paths in the present calculation. This process may give slightly different energy barriers for the atom-interchanging migration compared with static calculations to find the saddle points,

because potential-energy surfaces are formed by relaxing neighbouring atoms indifferently with respect to an atom fixed at each spatial point in static calculations. The migration energies for the atom-interchanging mechanism obtained in the present calculation, however, nearly agree with the energy differences between split and hexagonal configurations for Si^0 and between split and tetrahedral configurations for Si^{2+} in [17], while split configurations are close to the intermediate saddle configurations during the atom-interchanging migrations in the present calculation. If lattice relaxation is included rigorously by using a larger supercell geometry, a rigorous scheme for atom-interchange migration will be essential for accurate calculation where atom migration accompanies a large lattice relaxation.

The present calculations have revealed that the energy barrier for an atom-interchanging migration strongly depends on the migration path even when the self-interstitial moves between adjacent lattice sites, and that this energy barrier has a sharp peak around the saddle configuration during a migration process. A deviation from the saddle point causes a large lattice relaxation, resulting in a high or low energy barrier. A successive motion of a diffusing atom with a small migration step will be required for accurate energy-barrier calculations especially in the atom-interchanging process to elucidate mechanisms.

4.2. Migration mechanism

The theoretical values obtained in this study lie within those obtained by the above-mentioned experimental studies and the estimated values. The occurrence of a direct diffusion process does not contradict the experimental results under extrinsic conditions, where the self-interstitial density is extremely high. If the interstitial-interchange mechanism is mixed at some rate together with the direct-interstitial mechanism in the total diffusion procedure, it will account for the overall self-interstitial diffusion behaviour and oxidation enhancement of impurity diffusion. These considerations on the diffusion mechanism suggest that self-interstitial diffusion occurs as a combination of interstitial-interchange and direct-interstitial mechanisms for both Si^0 and Si^{2+}. The primary mechanism for individual cases is the interstitial-interchange or direct-interstitial mechanism for Si^0 and the direct-interstitial mechanism for Si^{2+} according to the present calculated results. The interstitial-interchange mechanism for Si^{2+} cannot, however, be excluded. This paper has extended the discussion on self-interstitial diffusion mechanisms only to n- and p-type silicon for simplicity. A Si^0 and Si^{2+} mixed diffusion will occur in actual cases, where the doping level is in the vicinity of the intrinsic condition. The migration energy is thought to decrease as a result of this combined mechanism. The basic mechanism remains, however, the same, as expected from the minimum barrier energy for various self-interstitial charged states.

Some correction in the obtained values for split and bond-centred configurations for Si^0 is needed for a rigorous calculation of migration energy, because the highest occupied states may have exceeded the band gaps. The cut-off energy has effects on the accuracy of the Hellmann–Feynman forces. The stable structure obtained by this force has been confirmed to deviate by about 0.1 eV from the actual stable structure. Atoms located on the supercell boundaries sometimes move slightly when a self-interstitial is moving from site to site, resulting in a small energy difference. The total energy error is, however, estimated to be at most 0.2 eV.

The present study is restricted on theoretical treatments of the relaxation from electronically excited states and of large semi-stable intermediate structures. Other types of self-interstitial migration mechanism may exist, but these are not covered by the present study. An interstitialcy-interchange mechanism through excited states or a larger deformed defect-modulated structure transport may be plausible mechanisms. Diffusion by these

mechanisms is expected to be rare because of their higher energy barriers [44]. Insofar as the present mechanism explains the overall aspects of experimental results, other mechanisms are left as future problems.

In recent years, theoretical work has been extended to various structures involving different atom species [32, 45, 46] and to dopant transport in silicon [33, 47]. Hydrogen diffusion has been intensely examined by both experimental and theoretical methods. Calculated diffusion coefficients for hydrogen in silicon agreed successfully with experiments [34, 48]. Since the hydrogen mass is far smaller than that of silicon, the migration energy will be of nearly the same order as the lattice vibration energy. Migration easily occurs without giving much relaxation to host sites. We do not face difficulties in obtaining an accurate migration energy by using a molecular dynamics method. Car–Parrinello molecular dynamics is a powerful technique for dealing with the migration of extremely light atoms [49]. It should, however, be noted here that the energy barriers for non-small atoms are far larger than the lattice vibration energy, and that molecular dynamics methods are not appropriate for such cases. This study was conducted to develop a method to find a critical path leading to a lowest-energy saddle configuration corresponding to the minimum migration barrier in general structures. This procedure is applicable to find minimum-energy barriers for atomic motion in solids, but we still need more care to find minimum barrier energies in general reaction processes when several atom motions initiate the total reaction process.

5. Conclusion

By searching for a critical path in the diffusion process, a total-energy density-function calculation has proposed silicon self-interstitial migration mechanisms involving paths and barrier energies in various ways. Calculations for Si^0 and Si^{2+} self-interstitials have revealed several stable configurations. The results suggest that self-interstitial diffusion occurs mainly as a combination of interstitial-interchange and direct-interstitial mechanisms by starting the migration from stable hexagonal and tetrahedral configurations. The interstitialcy-interchange mechanism, however, has been found to occur rarely, because the structure becomes unstable when an attempt is made to move it. The role of the interstitial-interchange mechanism is relatively large in the Si^0 case, while the direct-interstitial mechanism is more important in the Si^{2+} case. The calculated migration energies from 1.2 eV to slightly larger than 2 eV lie within widely ranging experimental results ranging from 0.13 eV to more than 2 eV obtained so far. Migrations with a relatively low energy barrier may be attributed to transition processes through bonds with successive bond formation during the process, or to direct diffusion steps of self-interstitials where the latter are loosely bound to adjacent atoms during the transition. The self-interstitial diffusion rates at low temperatures and the high or low interstitial diffusion rates at high temperatures are the results of various migration mechanisms and their calculated barrier energies.

Acknowledgments

The author would like to thank Dr K Ando for his continuous encouragement and helpful discussion, and Dr S Itoh and Mr I Ohmura for their technical support in designing the computational program code. The author also thanks Mr M Azuma for his encouragement.

References

[1] Fahey P, Griffin P B and Plummer J D 1989 *Rev. Mod. Phys.* **61** 289
[2] Watkins G D 1975 *Lattice Defects in Semiconductors 1974 (Inst. Phys. Conf. Ser. 23)* ed F A Huntley (Bristol: Institute of Physics) p 1
[3] Pantelides S T, Ivanov I, Scheffler M and Vigneron J P 1983 *Physica* B **116** 18
[4] Baraff G A, Schlüter M and Allan G 1983 *Physica* B **116** 76
[5] Car R, Kelly P J, Oshiyama A and Pantelides S T 1984 *Phys. Rev. Lett.* **52** 1814
[6] Pantelides S T, Oshiyama A, Car R and Kelly P J 1984 *Phys. Rev.* B **30** 2260
[7] Baraff G A and Schlüter M 1984 *Phys. Rev.* B **30** 3460
[8] Kelly P J and Car R 1992 *Phys. Rev.* B **45** 6543
[9] Mayer H J, Mehrer H and Maier K 1977 *Radiation Effects in Semiconductors 1976 (Inst. Phys. Conf. Ser. 31)* ed N B Urli and J W Corbett (Bristol: Institute of Physics) p 186
[10] Stolwijk N A, Schuster B and Hölzl J 1984 *Appl. Phys.* A **33** 133
[11] Tan T Y and Gösele U 1985 *Appl. Phys.* A **37** 1
[12] Taylor W, Marioton B P R, Tan T Y and Gösele U 1989 *Radiat. Eff. Defects Solids* **111** 131
[13] Mizuo S and Higuchi H 1985 *Appl. Phys. Lett.* **46** 587
[14] Kashio T and Kato K 1988 *Proc. Int. Conf. on Solid State Devices and Materials (Tokyo, 1988)* p 121
[15] Bar-Yam Y and Joannopoulos J D 1984 *Phys. Rev. Lett.* **52** 1129
[16] Bar-Yam Y and Joannopoulos J D 1984 *Phys. Rev.* B **30** 1844
[17] Bar-Yam Y and Joannopoulos J D 1984 *Phys. Rev.* B **30** 2216
[18] Brocks G, Kelly P J and Car R 1991 *Phys. Rev. Lett.* **66** 1729
[19] Mo Y W, Kleiner J, Webb M B and Lagally M G 1991 *Phys. Rev. Lett.* **66** 1998
[20] Vineyard G H 1957 *J. Phys. Chem. Solids* **3** 121
[21] Blöchl P E, Van de Walle C G and Pantelides S T 1990 *Phys. Rev. Lett.* **64** 1401
[22] Car R and Parrinello M 1985 *Phys. Rev. Lett.* **55** 2471
[23] Car R and Parrinello M 1987 *Solid State Commun.* **62** 403
[24] Paynne M C, Joannopoulos J D, Allan D C, Teter M P and Vanderbilt D H 1986 *Phys. Rev. Lett.* **56** 2656
[25] Stich I, Car R, Parrinello M and Baroni S 1989 *Phys. Rev.* B **39** 4997
[26] Hamann D R, Schlüter M and Chiang C 1979 *Phys. Rev. Lett.* **43** 1494
[27] Perdew J and Zunger A 1981 *Phys. Rev.* B **23** 5048
[28] Ceperley D M and Alder B J 1980 *Phys. Rev. Lett.* **45** 566
[29] Kleinman L and Bylander D M 1982 *Phys. Rev. Lett.* **48** 1425
[30] Ramchurn S K, Bird D M and Bullet D W 1990 *J. Phys.: Condens. Matter* **2** 7435
[31] Chadi D J and Cohen M L 1973 *Phys. Rev.* B **8** 5747
[32] Denteneer P J H, Van de Walle C G and Pantelides S T 1989 *Phys. Rev.* B **39** 10 809
[33] Nichols C S, Van de Walle C G and Pantelides S T 1989 *Phys. Rev.* B **40** 5484
[34] Van de Walle C G, Denteneer P J H, Bar-Yam Y and Pantelides S T 1989 *Phys. Rev.* B **39** 10 791
[35] Böer K W 1990 *Survey of Semiconductor Physics* (New York: Van Nostrand Reinhold)
[36] Taniguchi K and Antoniadis D A 1985 *Appl. Phys. Lett.* **46** 944
[37] Kump M R and Dutton R W 1988 *IEEE Trans. Comput.-Aided Design* **CAD-7** 191
[38] Bronner G B and Plummer J D 1987 *J. Appl. Phys.* **61** 5286
[39] Morehead F F 1987 *Defects in Electronic Materials (MRS Symp. Proc. 104)* ed M Stavola, S J Pearton and G Davies (Pittsburgh, PA: Materials Research Society) p 99
[40] Bronner G B and Plummer J D 1985 *Appl. Phys. Lett.* **46** 510
[41] Wada K, Inoue N and Osaka J 1983 *Defects in Semiconductors II* ed S Mahajan and J W Corbett (New York: North-Holland) p 125
[42] Mantovani S, Nava F, Nobili C and Ottaviani G 1986 *Phys. Rev.* B **33** 5596
[43] Seeger A, Föll H and Frank W 1977 *Radiation Effects in Semiconductors 1976 (Inst. Phys. Conf. Ser. 31)* ed N B Urli and J W Corbett (Bristol: Institute of Physics) p 12
[44] Pandey K C 1986 *Phys. Rev. Lett.* **57** 2287
[45] Besson M and Deleo G G 1991 *Phys. Rev.* B **43** 4028
[46] Zhang S B, Jackson W B and Chadi D J 1990 *Phys. Rev. Lett.* **65** 2575
[47] Nichols C S, Van de Walle C G and Pantelides S T 1989 *Phys. Rev. Lett.* **62** 1049
[48] Van de Walle C G, Bar-Yam Y and Pantelides S T 1988 *Phys. Rev. Lett.* **60** 2761
[49] Buda F, Chiarotti G L, Car R and Parrinello M 1989 *Phys. Rev. Lett.* **63** 294